**This paper is published as part of a *Dalton Transactions* themed issue on:**

# Thermoelectric Materials

Guest Editor Andrei Shevelkov
Moscow State University, Russia

Published in issue 4, 2010 of *Dalton Transactions*

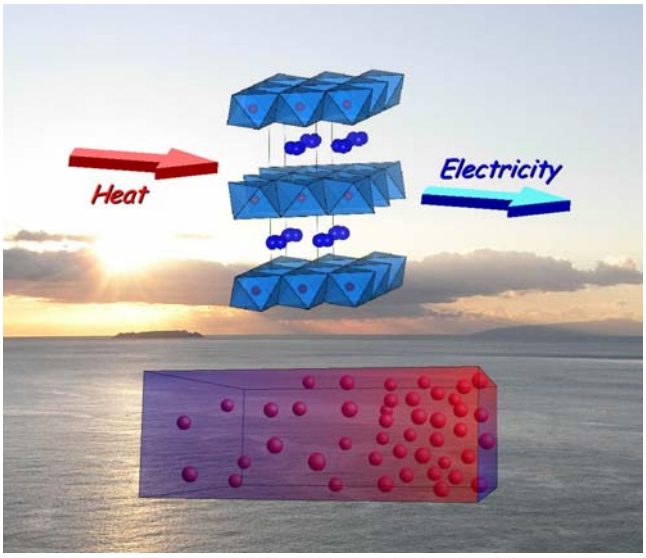


Image reproduced with permission of Ichiro Terasaki

Articles published in this issue include:

**PERSPECTIVES:**

Thermoelectric clathrates of type I
Mogens Christensen, Simon Johnsen and Bo Brummerstedt Iversen
*Dalton Trans.,* 2010, DOI: 10.1039/b916400f

Wet chemical synthesis and thermoelectric properties of V-VI one- and two-dimensional nanostructures
Genqiang Zhang, Qingxuan Yu and Xiaoguang Li
*Dalton Trans.,* 2010, DOI: 10.1039/b913462j

**HOT ARTICLES:**

Novel thermoelectric properties of complex transition-metal oxides
Ichiro Terasaki, Manabu Iwakawa, Tomohito Nakano, Akira Tsukuda and Wataru Kobayashi**,**
*Dalton Trans.,* 2010, DOI: 10.1039/b914661j

Effect of Zn doping on improving crystal quality and thermoelectric properties of borosilicides
Takao Mori, David Berthebaud, Toshiyuki Nishimura, Akiko Nomura, Toetsu Shishido and Kazuo Nakajima, *Dalton Trans.,* 2010, DOI: 10.1039/b916028k

Visit the *Dalton Transactions* website for more cutting-edge inorganic and organometallic research
www.rsc.org/dalton

# Wet chemical synthesis and thermoelectric properties of V-VI one- and two-dimensional nanostructures

**Genqiang Zhang, Qingxuan Yu and Xiaoguang Li***

***Received 7th July 2009, Accepted 17th November 2009***
***First published as an Advance Article on the web 9th December 2009***
**DOI: 10.1039/b913462j**



Recent advances in both theoretical and experimental studies on optimizing thermoelectric performance have proved to greatly benefit from nanostructure engineering. As a class of materials with the best thermoelectric properties near room temperature, V-VI alloy nanostructures, especially $Bi_2Te_3$ and its alloy with Sb, Se and so on, have attracted a broad interest. This perspective gives an overview of the progress in the wet chemical synthesis and property study of V-VI related one- and two-dimensional nanostructures. First, we discuss the preparation of one-dimensional nanowires/tubes, axial and radial modulated heterostructures, and two-dimensional platelet-like structures through various chemical routes. Then, we attempt to give a general outlook on the thermoelectric properties of V-VI single nanowires, and nanostructured films or bulk nanocomposites made of these chemically synthesized nanostructures. On the basis of the research in the synthetic methods and thermoelectric properties, the challenging issues and future research directions are briefly discussed. By no means is this a comprehensive coverage of V-VI related nanostructures, but a selection of those studies that could benefit the advance of thermoelectric properties of this material system in the near future.

## 1. Introduction

The world's demand for energy supply is causing a dramatic escalation of social and political unrest. Likewise, the environmental impact of the global climate change due to the combustion of fossil fuel is becoming increasingly alarming. These problems compel us to search for effective routes to build devices that can supply sustainable energy, with not only high efficiency but also environmental friendship. One way to relieve the energy crisis is to exploit devices based on renewable energy sources, such as solar energy, water power and so on. Another possible way to improve the sustainability of the electricity base is to recover the waste heat and convert it to electricity.[1] It is known that approximately 90 percent of the world's power is generated by heat engines through the combustion of fossil fuel. However, the use efficiency only ranges from 30 to 40 percent, which means that roughly 15 terawatts of heat is lost to the environment.[2] It is obvious that the fuel efficiency will be greatly enhanced if one can carry out the conversion of the waste heat to electricity, which may also solve the problems caused by the overuse of energy sources.

Thermoelectric (TE) devices, which consist of semiconductor materials that can directly convert thermal energy to electricity and *vice versa*, provide an alternative route to transform the above mentioned waste heat to useful electric power.[3,4] To build TE modules with high efficiency will be the critical milestone for practical applications of TE materials. Unfortunately, TE materials have

*Hefei National Laboratory for Physical Sciences at Microscale, Department of Physics, University of Science and Technology of China, Hefei, 230026, P. R. China. E-mail: lixg@ustc.edu.cn; Fax: +86-551-3603408; Tel: +86-551-3603408*

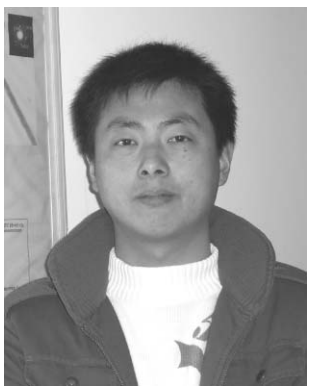

**Genqiang Zhang**

*Genqiang Zhang received his BS degree in materials chemistry in 2004 and PhD degree in condensed matter physics in 2009, both from the University of Science and Technology of China supervised by Prof. Xiaoguang Li. He is interested in the solution phase synthesis, property study and device applications of nanostructured thermoelectric materials.*

**Qingxuan Yu**

*Qingxuan Yu received his PhD in 1994 from Shanghai Institute of Microsystem and Information Technology, Chinese Academy of Sciences, then joined the Department of Physics at the University of Science and Technology of China as an associate professor in 1997. His research interests include the synthesis of nanostructured materials and fabrication of semiconductor devices.*

long been too inefficient to be cost-effective for fully scalable applications in our daily life. Therefore, the central issue in the TE area is still to optimize the material performances, which is defined as a dimensionless TE figure of merit, $ZT = S^2\sigma T/\kappa$, where $S$, $\sigma$, $T$ and $\kappa$ are the Seebeck coefficient, electrical conductivity, temperature, and thermal conductivity respectively. Two different approaches have been taken for developing high performance TE materials: one is to exploit new families of advanced bulk materials with a high $ZT$ value, such as the partially filled skutterudites based on alloys of $CoSb_3$; the other is to further enhance the currently promising TE materials using nanotechnology,[5-9] because it is predicted that the introduction of nanoscale constituents would induce quantum-confinement effects to enhance the power factor $S^2\sigma$. In addition, the internal interfaces formed in nanostructures may reduce the thermal conductivity ($\kappa$) more than the electrical conductivity ($\sigma$) based on differences in their respective scattering lengths, which benefits the enhancement of the $ZT$ value. For example, Venkatasubramanian's group successfully fabricated high quality V-VI alloy related superlattice films and obtained a much higher $ZT$ value when compared with corresponding bulk samples.[7-9]

As a class of the most widely used commercial TE materials near room temperature,[4] V-VI alloys, especially $Bi_2Te_3$ and its alloy with Sb, Se and so on, could be applicable for large-scale energy conversion after further optimizing their $ZT$ value and have been broadly studied. In this article, we discuss the latest advance in wet chemical synthesis and property study of V-VI based TE nanostructures, especially for the one- and two-dimensional nanoarchitectures. This perspective is mainly composed of two parts. In the first part, the syntheses of V-VI nanostructures including one-dimensional nanowires, nanotubes, axial and radial modulated heterostructures and two-dimensional platelets through various chemical routes are discussed. In the second part, we introduce the TE properties of single nanowire, nanostructured thin films and bulk nanocomposites composed of these nanostructures. At the end, we will give a summary and outlook on the active research topics on V-VI related nanostructures based on the analysis of synthesis and property study parts.

**Xiaoguang Li**

*Xiaoguang Li received his PhD in 1991 from the Institute of Solid State Physics, Chinese Academy of Sciences. He worked at the University of Tokyo as a JSPS Research Fellow from 1993 to 1994. He became a faculty member in the University of Science and Technology of China as a full professor in 1993. Research interests include synthesis, microstructure, physical properties and prototype of the related devices for transitional metal oxides and nanostructured thermoelectric materials.*

## 2. Chemical synthesis of V-VI TE nanostructures

### 2.1 Nanowires

TE nanowire systems have attracted intense interest because of their possible applications in high efficiency nanodevices. The strong two-dimensional (2D) confinement in such a system could benefit the $ZT$ enhancement in the following aspects:[10-12] (i) an increase in Seebeck coefficient ($S$) derived from the increasing density of state in the vicinity of the Fermi level, (ii) a suppressed thermal conductivity ($\kappa$) due to the stronger phonon boundary scattering without an appreciable increase in electron-boundary scattering, and (iii) an increase in the carrier mobility at a given concentration due to the size quantization effect. As for the synthesis of V-VI nanowires, the most effective routes are wet chemical synthesis, including electrodeposition into anodic aluminium oxide (AAO) or polycarbonate (PC) template, and various solution based methods.

**2.1.1 Electrodeposition method for V-VI nanowires.** The electrodeposition method is one of the most cost-effective techniques for the fabrication of nanostructured materials, especially for the nanowires combined with highly ordered porous templates. This method possesses various advantages compared with other synthetic routes, including room temperature operation, low-equipment cost, no vacuum required, high deposition rates and easy scalability. There have been various studies on the fabrication of V-VI related nanowires through this method. The first report comes from the Martin group on the galvanostatic electrodeposition of $Bi_2Te_3$ nanowires with polycrystalline nature and no obvious preferential orientation using $Bi(NO_3)_3{\cdot}5H_2O$ and Te powder as source materials.[13] In recent years, along with an advance in the electrodeposition technique and the fabrication of the AAO template, both the quality and category of the samples, have made a great progress and many kinds of V-VI alloy nanowires with single crystalline nature and well oriented growth direction have successfully been obtained. For example, single crystalline $Bi_2Te_3$ nanowires with <110> growth direction were obtained through the potentiostatic electrodeposition at –0.46 V *vs.* $Hg/HgSO_4$ (in saturated $K_2SO_4$) with a three-electrode configuration consisting of a reference electrode, a Ag sputtered alumina template as a working electrode and a Pt gauze as the counter electrode in an ice bath with concentrations of 0.075 M $Bi^{3+}$ and 0.1 M Te in 1 M $HNO_3$.[14-16] In addition, the filling efficiency of the AAO template reached about 80%. Our group developed a simple galvanostatic electrodeposition process for the synthesis of Bi, $Bi_2Te_3$ and $Sb_2Te_3$ nanowire arrays from aqueous electrolyte at room temperature, as shown in Fig. 1, with single crystalline nature, highly oriented growth direction and almost 100% filling efficiency of the pores.[17-19] The electrolyte solution for the Bi nanowire deposition consists of 100 g $L^{-1}$ Bi $(NO_3)_3{\cdot}5H_2O$, 120 g $L^{-1}$ glycerol, 50 g $L^{-1}$ tartaric acid and 40 g $L^{-1}$ $KNO_3$. The pH of the solution was adjusted to 2 by the addition of nitric acid. For the $Bi_2Te_3$ nanowire synthesis, the electrolyte solution contains 0.035 M $Bi(NO_3)_3{\cdot}5H_2O$, and 0.05 M $HTeO_2^+$ came from the reaction of Te powder with 5 M $HNO_3$. The final pH value of the solution is tuned to 1 through nitric acid. The preparation of $Sb_2Te_3$ electrolyte solution is similar to those of Bi and $Bi_2Te_3$ syntheses. However, it should be noted that for the synthesis of the high quality $Sb_2Te_3$ nanowire, the formation of Sb-citric complex

 

was necessary by dissolving $SbCl_3$ with citric acid and potassium citric in order to obtain a stable electrolyte.[19] These studies also indicate that it is possible to obtain various V-VI nanostructures with tunable compositions, sizes and crystallinity for unitary and binary V-VI nanowires through facile electrodeposition method. Recently, it has been reported that the microstructure of the $Bi_2Te_3$ nanowires strongly depends on the different growth mechanism derived from different electrochemical process, *i.e.* galvanostatic, potentiostatic and pulsed electrodeposition.[20] Compared with the well developed unitary and binary V-VI nanowire electrodeposition technique, the fabrication for complex ternary nanowires is relatively undeveloped. Until now, although some ternary alloy nanowires, including $(Bi_{1-x}Sb_x)_2Te_3$ and $Bi_2Te_{3-y}Se_y$ with different $x$ or $y$ contents could be obtained,[21-23] the quality of the samples is not as perfect as that of binary V-VI alloy nanowires.

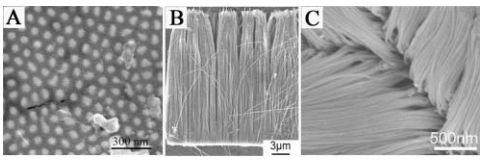


**Fig. 1** SEM images of Bi, $Bi_2Te_3$ and $Sb_2Te_3$ nanowires through the galvanic electrodeposition method combined with AAO template.[17-19]

**2.1.1 Solution phase synthesis of V-VI nanowires.** The solution phase method has proved to be an effective and powerful strategy for controllable synthesis of various nanostructures with tunable morphologies and sizes, which have been systematically indicated in several review articles.[24-28] Compared to the template assisted electrodeposition method, solution phase methods have features on large-scale production, no template removal step, and better dispersion in the liquid medium, and so on. More importantly, it is relatively easier to obtain thin diameter nanowires, which may strongly contribute to the improvement of TE performance.

For example, the Bi nanowires with a mean diameter of 5.9 ± 2.4 nm and lengths up to 5 μm, as shown in Fig. 2A, have been obtained through the high-temperature thermal decomposition of $Bi[N(SiMe_3)_2]_3$ in the presence of poly(1-hexadecene)$_{0.67}$-co-(1-vinylpyrrolidinone)$_{0.33}$ and $NaN(SiMe_3)_2$.[29-30] In order to obtain binary $Bi_2Te_3$ nanowires, Buhro *et al.* synthesized uniform Te nanowires from $TeCl_4$ and trioctylphosphine oxide (TOPO) in polydecene at 250 °C, followed by the reaction of Te nanowires with $BiPh_3$ at 160 °C. The obtained $Bi_2Te_3$ nanowires exhibited a

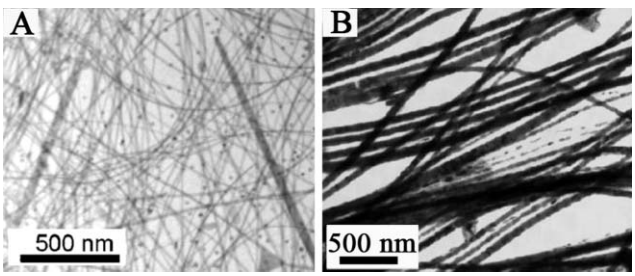


**Fig. 2** TEM images of (A) Bi nanowires synthesized at 203 °C in the presence of poly(1-hexadecene)$_{0.67}$-co-(1-vinylpyrrolidinone)$_{0.33}$ and $NaN(SiMe_3)_2$; (B) $Bi_2Te_3$ nanowires by reaction of $BiPh_3$ and Te nanowires at 160 °C.[29]

<001> growth direction and had an average diameter of 67.8 ± 17.0 nm, as shown in Fig. 2B.[29] In addition, Li's group obtained single crystalline Bi nanowires with <001> growth direction by reducing sodium bismuthate ($NaBiO_3 \cdot 2H_2O$) with ethylene glycol in the presence of poly(vinyl pyrrolidone) (PVP) using a solvothermal process.[31]

In addition, a modified polyol process was recently developed for the high-yield synthesis of single crystalline Bi nanowires by refluxing ethylene glycol solvent with an appropriate amount of $BiCl_3$, PVP and NaOH at 190 °C for about 60 min.[32] In this so-called polyol process, ethylene glycol serves as both solvent and reducing agent and the involved reaction processes can be described as follows:[32]

$$BiCl_3 + 3NaOH \xrightarrow{\Delta} Bi(OH)_3 \downarrow + 3NaCl$$

$$Bi(OH)_3 + NaOH \xrightarrow{\Delta} NaBiO_2 + 2H_2O$$

$$HOCH_2\text{-}CH_2OH \xrightarrow{\Delta} CH_3CHO + H_2O$$

$$3CH_3CHO + 2NaBiO_2 \xrightarrow{\Delta} 2CH_3COONa + CH_3COOH + 2Bi + H_2O$$

Aqueous-phase solution method has also proved to be a feasible route for the synthesis of V-VI alloy nanowires by Ramanath's group.[33] They developed a facile low temperature refluxing approach for synthesizing single crystal $Bi_2Te_3$ nanorods with diameters in the range of 27–130 nm.[33] They utilized orthotelluric acid and anhydrous bismuth chloride as precursors, thioglycolic acid or L-cysteine as the complexing agent for $Bi^{3+}$ ions in aqueous medium, and hydrazine monohydrate as the reducing agent. The well crystalline $Bi_2Te_3$ nanorods were obtained after refluxing the precursor solution at 100 °C for 5 h. In addition, Sun *et al.* reported an alternative aqueous synthesis of $Bi_2Te_3$ nanowires with average diameters of 10–20 nm and lengths up to about 1 μm. The nanowire products could be obtained at 65 °C for 48 h using Te powder and $BiCl_3$ as precursors, sodium dodecyl-benzenesulfonate (SDBS) as a surfactant, and $NaBH_4$ as a reductant.[34]

## 2.2 Nanotubes

TE nanotubes have been considered as a more promising nanostructure compared with solid nanowires. This is because of the stronger phonon blocking effect derived from their structure feature of both low-dimensionality and hollow tube channels, which could result in the reduced lattice thermal conductivity and different electronic transport behaviors as compared with those of nanowires.[35-36] Therefore, it will be quite important to develop effective routes for synthesizing tubular nanostructures of TE materials in order to study their promising properties.

**2.2.1 Electrodeposition method for V-VI nanotubes.** As a powerful route for synthesizing nanowires, the electrodeposition method has proved to be an appropriate method for the synthesis of the V-VI nanotubes through the optimized procedures with the AAO template. In order to obtain nanotubes, the AAO template with a mesh-like Au layer onto one planar surface was firstly formed according to the procedures schematically illustrated in Fig. 3. Li *et al.*[37,38] demonstrated the synthesis of Sb and Bi nanotubes by electrodeposition into nanochannels of the template with a mesh-like Au layer. Based on this work, Bi nanotubes with predesigned thickness could be reached by tuning the thickness of the sputtering Au layer and the applied current density during the electrodeposition process,[39] which may contribute to the

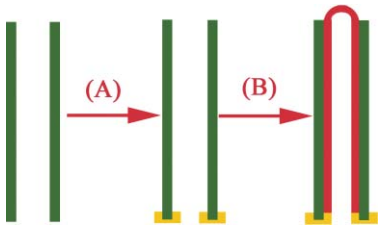


**Fig. 3** Schematic procedure for the synthesis of Bi nanotubes through electrodeposition process. (A) Sputtering a mesh-like Au layer on one planar surface side of the AAO template and (B) electrodeposition of Bi nanotubes.[37]

follow-up study of their size-dependent electrical and thermal transport properties. This synthetic route was further extended to synthesize the binary and ternary V-VI nanotubes, including $Bi_2Te_3$ and $Bi_2Te_3$ derived alloys such as the n-type $Bi_2Te_{3-y}Se_y$ and p-type $Bi_{2-x}Sb_xTe_3$ tubular nanostructure by adjusting the electrolyte solution.[40] The outer diameter and thickness of the nanotubes are about 200 nm and 40–70 nm, respectively. It should be noted that the large pore diameter (~200 nm) of the used AAO template is a necessary precondition to obtain tubular structure while only nanowires can be synthesized when the pore diameter was reduced to 50–60 nm.[40] In addition, the nanotube products were polycrystalline, and the diameter of the nanotubes was not well controlled.

Although several kinds of V-VI nanotube fabrication have been achieved through the above-mentioned electrodeposition process, it is still a challenge to carry out the controllable synthesis of high quality V-VI nanotubes, especially the binary and ternary alloy nanotubes which may possess more promising TE properties. Therefore, much effort needs to be devoted to optimize the current electrodeposition techniques in order to synthesize single crystalline nanotubes with controllable sizes.

**2.2.2 Solution phase synthesis of V-VI nanotubes.** The effective syntheses of V-VI TE nanotubes through solution phase methods are not well developed at present as compared with those of nanowires, although Bi, $Bi_2Se_3$ and $Bi_2Te_3$ nanotubes have been obtained through hydro-/solvothermal processes, aqueous chemical syntheses, galvanic replacement reactions, and solution phase nanoscale Kirkendall effect fabrication methods.[41-45]

As a powerful route for various nanostructures,[46,47] hydrothermal method has been applied to synthesize the V-VI tubular nanostructures. For example, thin Bi nanotubes with diameters of about 5 nm and lengths up to 0.5–5 μm could be obtained through a low-temperature hydrothermal reduction of $Bi(NO_3)_3$ with aqueous hydrazine solution at 120 °C.[41] The chemical reaction can be formulated as:

$$N_2 + 4H_2O + 4e \rightarrow N_2H_4 + 4OH^- \ (E^0 = -1.16\ V)$$

$$Bi(OH)_3 + 3e \rightarrow Bi + 3OH^- \ (E^0 = -0.46\ V).$$

Binary $Bi_2Te_3$ nanotubes were also obtained through the hydrothermal process using $BiCl_3$ and Te powder as precursors, ethylenediaminetetraacetic disodium salt (EDTA) and NaOH as additives, and $NaBH_4$ as the reducing agent.[42,43] However, these processes still have some limitations, such as low nanotube production yield and the polycrystalline nature of the products which could play a negative effect on enhancing the TE performance.

Xiao *et al.* recently reported a facile strategy on the basis of the galvanic replacement reaction of $Bi^{3+}$ and $HTeO_2^+$ ions with Ni nanowires, as shown in Fig. 4, for synthesizing $Bi_2Te_3$ nanotubes with high yield production.[44] This facile route solved the low nanotube production yield limitation involved in previous reports, and the aspect ratio and composition of the nanotubes were controllable too. However, this method still has the limitation in the polycrystalline nature of the products, as shown in Fig. 5, which could lead to the decrease of the electrical conductivity.

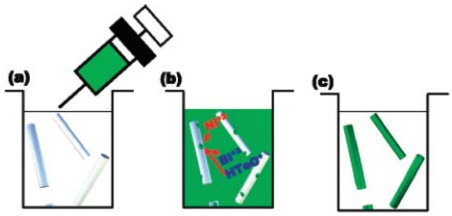


**Fig. 4** Schematic illustration of $Bi_2Te_3$ nanotube synthesis through galvanic replacement reaction between $Bi^{3+}/HTeO_2^{2+}$ and Ni nanowires.[44]

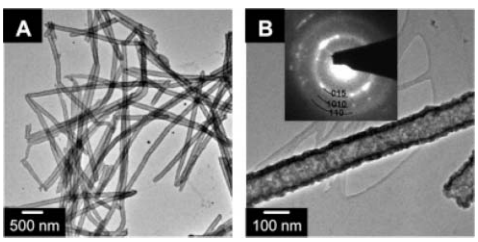


**Fig. 5** TEM images and SAED pattern of the $Bi_2Te_3$ nanotubes synthesized from Ni nanowires. (A) Low-magnification TEM image; (B) an individual $Bi_2Te_3$ nanotube and the corresponding SAED pattern.[44]

Our group developed an ethylene glycol mediated solution phase method for the synthesis of large scale, single crystalline $Bi_2Te_3$ nanotubes.[45] In a typical synthesis, Te nanowires with <001> growth direction were firstly obtained by reducing $TeO_2$ dissolved in ethylene glycol through $N_2H_4{\cdot}H_2O$ followed by the addition of Bi precursor solution. Well crystalline $Bi_2Te_3$ nanotubes as shown in Fig. 6 can be formed after 20 min at 160 °C. By careful observation of the time dependent products during the shape evolution from solid Te nanowires to $Bi_2Te_3$ nanotubes, as shown in Fig. 7, it is safe for us to infer that the nanoscale Kirkendall effect could be the involved mechanism. The formation process is schematically illustrated in Fig. 8, which can be described as follows: firstly, the Bi atoms selectively nucleate at the side surfaces of the Te nanowires, which subsequently results in the formation of core/shell nanowires (Step I in Fig. 8). After reacting for about 4 min, the formation of the Bi–Te alloy layer can be observed (Step II in Fig. 8) and the non-reciprocal diffusion between Bi and Te through the Bi–Te alloy layer leads to the void formation between the Bi–Te alloy layer and the core Te nanowires, as shown in Step III in Fig. 8. The continuous mass transformation could be maintained through the bridge structure indicated in Step IV of Fig. 8, similar to the formation of hollow nanoparticles by the Kirkendall effect.[48-50] The Te core nanowire disappeared when the reaction time reaches about 10 min and the well crystallized $Bi_2Te_3$ nanotubes were obtained after reacting for about 20 min.[45] This work has several advantages including the single crystalline

 

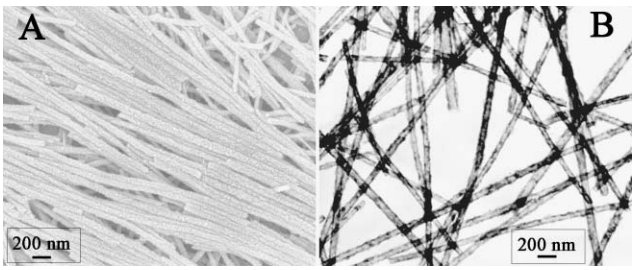


**Fig. 6** SEM and TEM images of single crystalline $Bi_2Te_3$ nanotubes through the solution phase nanoscale Kirkendall effect.[45]

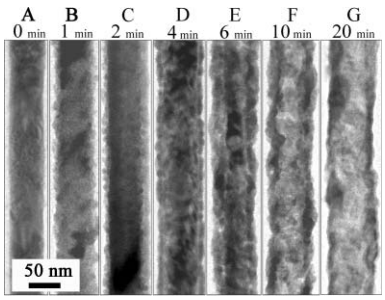


**Fig. 7** TEM images of the time-dependent products during the formation of $Bi_2Te_3$ nanotubes after the injection of Bi precursor to Te nanowire containing solution.[45]

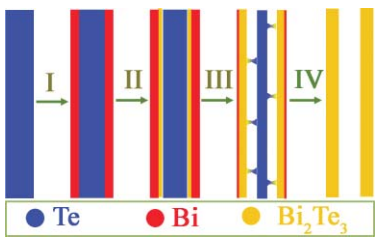


**Fig. 8** Schematic illustration of the shape evolution process from Te nanowire to $Bi_2Te_3$ nanotube.[45]

nature of the products, high-yield production, totally controllable sizes through adjusting the Te nanowire diameters and easily scalable applications for the synthesis of ternary or quaternary alloy nanotubes.

### 2.3 One-dimensional (1D) heterostructures

The formation of heterostructures in 1D nanostructures is of particular significance with respect to their potential applications as building blocks for various nanodevices.[51-58] V-VI related TE heterostructures, including axial modulated superlattice or multilayered nanowires and radial modulated core/shell nanowires, have also attracted intense interest because of their possibly more effective optimization on the TE performance.[36,59-60] Compared with simple nanowires, the heterostructure interfaces between every two adjacent segments in superlattice or multilayered nanowires, or between core and shell in core/shell nanowires, may further reduce the lattice thermal conductivity by blocking the phonon scattering along the wire axis, while the electrical conduction may be sustained.[36,59-60] At the current stage, the central issue is still to exploit effective routes for synthesizing high quality heterostructure nanowires, followed by studying their properties in the near future.

**2.3.1 Electrodeposition method for V-VI related superlattice nanowires.** With the development of vapor phase deposition techniques, various heterostructure nanowires with axial or radial modulated compositions related to Si, Ge, III–V based compounds and so on, have been realized by combing the vapor–liquid–solid (VLS) mechanism with a heteroepitaxial growth process.[51-58] However, for the synthesis of V-VI related superlattice or multilayered nanowires, the pulsed electrodeposition method combined with porous templates, until now, is still the most effective strategy. For example, single crystalline Bi/Sb superlattice nanowires were synthesized in AAO templates by means of a pulsed electrodeposition technique in a single ethanol electrolyte consisting of 0.01 M $BiCl_3$, 0.08 M $SbCl_3$, 0.2 M $H_3BO_3$, 0.01 M $C_4H_6O_6$ and 0.1 g of $CH_3(CH_2)_{11}SO_3Na$ with a pH value of 2.[61] The lengths of Bi and Sb segments could be modulated in the range of 13–350 nm and 13–325 nm (Fig. 9A-D), respectively, through adjusting the deposition time, deposition potential and the concentrations of $Bi^{3+}$ and $Sb^{3+}$ ions in the electrolyte.[61] Subsequently, Dou *et al.* extended the pulsed electrodeposition method to synthesize single crystalline $Bi/Bi_{0.5}Sb_{0.5}$ superlattice nanowires in the electrolyte composed of 0.04 M $L^{-1}$ $BiCl_3$, 0.08 M $L^{-1}$ $SbCl_3$, 40 g $L^{-1}$ tartaric acid, 50 g $L^{-1}$ citric acid, 100 g $L^{-1}$ glycerol, 70 g $L^{-1}$ NaCl and 1.0 M $L^{-1}$ HCl with a pH value of 0.82.[62]

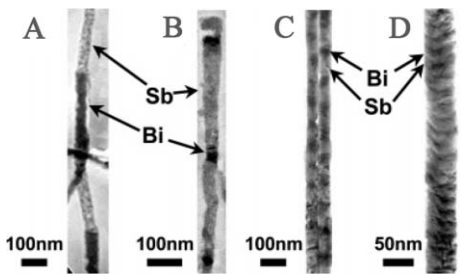


**Fig. 9** TEM images of Bi/Sb superlattice nanowires with different lengths of Bi and Sb segments modulated by changing the deposition time $t_{Sb}$ and $t_{Bi}$, deposition potential $V_{Sb}$ and $V_{Bi}$, and the concentration of $Bi^{3+}$ and $Sb^{3+}$ ions in electrolyte.[61]

As one of the best TE materials near room temperature, the fabrication of $Bi_2Te_3$ and its derived alloys related superlattice or multilayered nanowires will be of great significance to further optimize their TE performances for possible scalable applications, where much attention has been paid. Xiao *et al.* utilized a potentiostatic electrodeposition into polycarbonate templates for the synthesis of $Bi_2Te_3/(Bi_{0.3}Sb_{0.7})_2Te_3$ multilayered nanowires, as shown in Fig. 10, from a single bath containing 0.1 mM $Bi^{3+}$, 0.7 mM $HTeO_2^+$, 1.6 mM $SbO^+$, 33 mM tartaric acid and 1 M nitric acid.[63] In this method, a waveform potential profile was applied between −20 and −100 mV *vs.* SCE (saturated calomel electrode) for $Bi_2Te_3$ and $(Bi_{0.3}Sb_{0.7})_2Te_3$ segment, respectively. The composition and length of each segment are tunable by adjusting deposition potentials and time. Our group recently reported an indepth study on the synthesis of $Bi_2Te_3$/Sb multilayered nanowires (Fig. 11) through an AAO template-assisted pulsed electrodeposition technique.[64] The electrolyte solution was prepared by dissolving 0.012 M $TeO_2$ into 2 M $HNO_3$ solution, followed by adding 1 M $C_6H_8O_7{\cdot}H_2O$, 0.5 M $K_2C_6H_5O_7{\cdot}H_2O$ and 0.004 M $Bi(NO_3)_3{\cdot}5H_2O$. Finally, 0.1 M $Sb_2O_3$ was dissolved in the

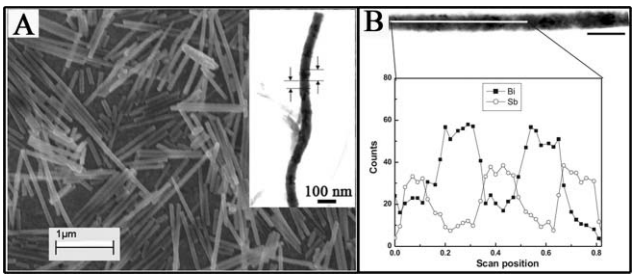


**Fig. 10** (A) SEM and TEM (inset) images of the multilayered $Bi_2Te_3/(Bi_{0.3}Sb_{0.7})_2Te_3$ nanowires after the removal of polycarbonate template, and (B) EDS line scan for showing compositional oscillations of Sb and Bi in an individual $Bi_2Te_3/(Bi_{0.3}Sb_{0.7})_2Te_3$ multilayered nanowire.[63]

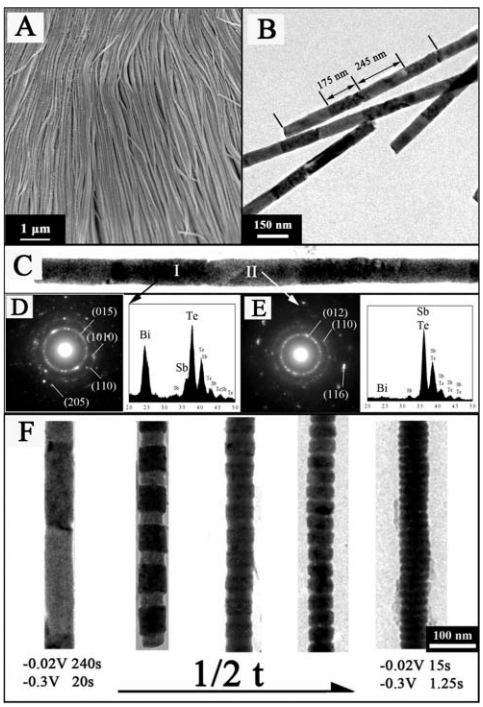


**Fig. 11** (A) SEM and (B, C) TEM images of the $Bi_2Te_3$/Sb multilayered nanowires, SAED pattern and corresponding EDS results for (D) segment I and (E) segment II, (F) the comparison of the corresponding five kinds of $Bi_2Te_3$/Sb multilayered nanowires deposition with different times.[64]

above solution by heating. Fig. 11A-E show the morphology and microstructure analyses of the $Bi_2Te_3$/Sb multilayered nanowires obtained under the conditions of –0.02 V (*vs.* Ag/AgCl) 240 s for the $Bi_2Te_3$ segment and –0.3 V (*vs.* Ag/AgCl) 20 s for the Sb segment. More importantly, the length of each segment could be precisely controlled as shown in Fig. 11F, and the minimum period of the segments for the products reached about 10 nm through manipulating the deposition time to 15 s for $Bi_2Te_3$ and 1.25 s for the Sb segment, which may greatly benefit the TE properties of these nanowires.

However, these two studies about the synthesis of $Bi_2Te_3$ related multilayered nanowires have a common disadvantage that the obtained products are polycrystalline, which may decrease the electrical conductivity and inhibit the enhancement of the $ZT$ value of the nanowires although the lattice thermal conductivity could be reduced. Therefore, it will be of great significance to exploit effective routes for $Bi_2Te_3$ related multilayered nanowires with the single crystalline nature. Recently, we developed a convenient route for the spontaneous formation of $Bi_2Te_3$/Te multilayered nanowires in which each segment was single crystalline, as shown in Fig. 12, using the precipitation reaction of the supersaturated $Bi_{0.26}Te_{0.74}$ alloy nanowires in a nanoconfined system.[65] In a typical synthesis, the supersaturated $Bi_{0.26}Te_{0.74}$ nanowires were firstly obtained through a simple galvanostatic electrodeposition into the AAO template in the aqueous electrolyte containing 50 mM $HTeO_2^+$ and 12.5 mM $Bi^{3+}$ ions. Then the template with the nanowires was post-annealed at 300 °C in an evacuated silica tube to form the multilayered $Bi_2Te_3$/Te heterostructure nanowires. On the basis of the careful analysis of the differential scanning calorimetry (DSC) and X-ray diffraction results of the supersaturated $Bi_{0.26}Te_{0.74}$ nanowires after annealed at different temperatures (Fig. 13), one can find that the phase transformation process happens at the temperature range from 120 °C to 140 °C. Guided by this, the results of the control samples annealed under different conditions indicate that the formation process of the heterostructure nanowires can be regarded as the classical precipitation in the alloy system (Fig. 14), which consists of three stages, *i.e.*, the nucleation of Te crystals from supersaturated $Bi_{0.26}Te_{0.74}$ nanowires at elevated temperature; the growth of the Te nuclei by absorbing Te atoms along with the aging time increases; and the formation of the block-to-block structure due to the confined effect of the nanochannel during the Te crystal growth.[65] This study provides a facile and extendable strategy for synthesizing heterostructure nanowires, which has been successfully applied in the synthesis of CdTe/Te multilayered nanowires.[66]

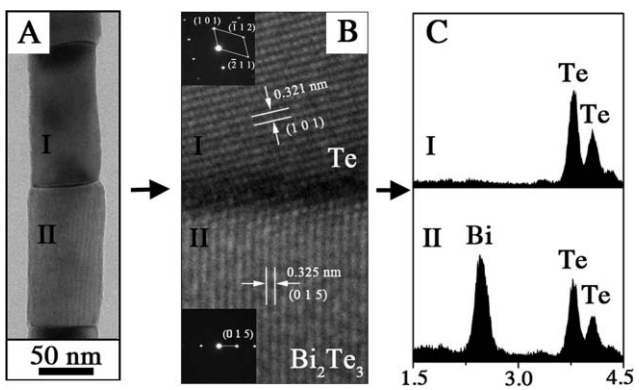


**Fig. 12** Microstructure and composition analyses of $Bi_2Te_3$/Te multilayered heterostructure nanowires through confined precipitation: (A) close up of a couple of segments, (B) HRTEM image and corresponding SAED patterns and (C) the EDS spectrum of each segment in (A).[65]

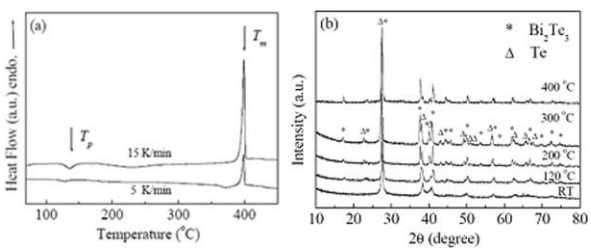


**Fig. 13** (a) DSC results of the as-deposited Bi–Te nanowire arrays with different heating rates. (b) Powder XRD patterns of the as-deposited and annealed supersaturated Bi–Te nanowires at different temperatures.[65]

 

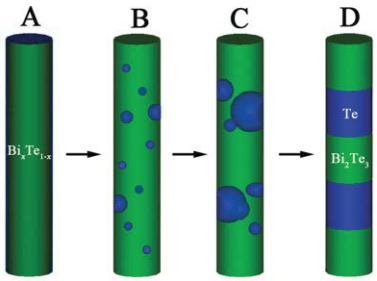


**Fig. 14** Schematic illustration of the formation process of $Bi_2Te_3$/Te heterostructure nanowires.[65]

**2.3.2 Solution phase method for V-VI related 1D heterostructures.** As an alternative route for heterostructure nanowires, a solution phase method has been well developed to synthesize both axial and radial modulated semiconductor heterostructure nanowires.[67-70] However, to the best of our knowledge, there is still no reports on the synthesis of V-VI related axial heterostructure nanowires, where much effort should be devoted. On the other hand, the synthesis of V-VI radial modulated heterostructure nanowires is also a great challenge although there have been limited studies on this area. For example, Lu *et al.* developed a two-step epitaxial growth of the cylindrical strings of $Bi_2Te_3$ platelets on the surface of the Te rod by packing them along the *c*-axis in a top-bottom-top-bottom sequence through a high-temperature organic solution approach.[71] Whereas, for V-VI core/shell nanowires, previous reports gave no appropriate route until recently. Our group successfully developed a facile EG mediated solution phase epitaxial growth of core/shell Te/Bi and Te/$Bi_2Te_3$ heterostructure nanowires using Te nanowires as the *in situ* templates for the subsequently epitaxial growth of Bi shells.[72] In a typical synthesis, well dispersed single crystalline Te nanowires were firstly obtained by reducing $TeO_2$ dissolved in EG at 170 °C using $N_2H_4{\cdot}H_2O$ as a reducing agent and PVP as an organic additive. Then the Bi precursor solution consisted of $Bi(NO_3)_3{\cdot}5H_2O$ and $H_2C_2O_4$ was injected into the Te nanowire solution followed by the addition of another appropriate amount of $N_2H_4{\cdot}H_2O$. The diameter and length of the obtained core/shell nanowires are uniform, as shown in Fig. 15A and B, which are about 20–25 nm and 1.5–2 μm, respectively. The epitaxial relationship between Te and Bi can be clearly indicated through the HRTEM images taken from an individual core/shell nanowire (Fig. 15C–F), which can be described as: Te (100)//Bi (100) and Te <001>//Bi <001>. It should be noted that the diameter of the core nanowire is about 18–20 nm and the thickness of the shell is only about 2–5 nm. This feature could benefit the optimization of the TE properties of the product. This solution phase synthesis of V-VI related core/shell heterostructures could be extended to other material systems.[72]

## 2.4 Two dimensional (2D) platelet-like nanostructure

Besides various 1D nanostructures, V-VI related 2D platelet-like nanostructures have attracted intense interest too. Various solution phase methods, including the high-temperature organic solution route, hydro-/solvothermal processes, microwave assisted chemical syntheses, and so on, have recently been developed to synthesize this kind of nanostructure.[73-77] For example, well defined $Bi_2Te_3$ hexagonal platelets were synthesized through

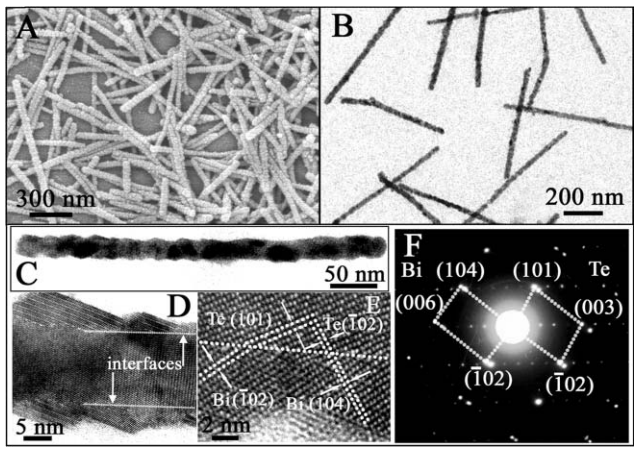


**Fig. 15** Morphology and microstructure analyses of Te/Bi core/shell heterostructure nanowires: (A) SEM, (B, C) TEM images, (D, E) HRTEM images and (F) corresponding SAED pattern taken from the single nanowire in (C).[72]

a high-temperature organic solution process using bismuth-2-ethylhexanoate and Te in trioctylphosphine (TOP) as precursors.[71] The generation of $Sb_2Te_3$ platelets could be achieved through a single-source precursor-$Sb[(TePiPr_2)_2N]_3$ using the aerosol-assisted chemical vapor deposition at 375–475 °C.[73]

The hydro-/solvothermal process has been regarded as an effective method for the synthesis of V-VI platelet-like nanostructure. Wang *et al.* and Shi *et al.* obtained $Sb_2Te_3$ hexagonal platelets through solvothermal and hydrothermal routes, respectively, using inorganic $SbCl_3$, Te powder or $K_2TeO_3$ as precursors.[74,75] In addition, a microwave-assisted wet chemical route was also reported to be appropriate to synthesize $Sb_2Te_3$ hexagonal platelets using antimony sodium tartrate ($Na(SbO)C_4H_4O_6$) and Te powder as precursors.[76] Although the advance of the synthetic routes for binary V-VI platelet-like nanostructures, the precise formation mechanism is still not well established in these studies. In addition, it's unclear whether the ternary V-VI platelets could be carried out through the above mentioned strategies.

Considering the similar crystal structure and anisotropic bonding environment of the V-VI related materials, it could be possible to build this class of materials into the platelet-like morphology in a unified system. To reach this goal, our group developed a simple solvothermal approach for synthesizing not only binary $Bi_2Te_3$, $Sb_2Te_3$ and $Bi_2Se_3$ but also ternary $Bi_2Te_2Se$ and $BiSbTe_3$ alloy hexagonal platelets using convenient oxides as source materials and nontoxic EG as reducing agent.[77] More important, the formation mechanism of the hexagonal platelet-like structure was systematically studied through the observation of the time-dependent products during the formation of $Bi_2Te_3$ platelets, as shown in Fig. 16. The oriented attachment mechanism was found to be responsible for the growth of hexagonal platelets, which could be concluded as follows: (i) reduction of $Bi_2O_3$ and $TeO_2$ to Bi and Te atoms by EG; (ii) dissolving Bi and Te crystals and the subsequent formation of Bi–Te alloy particles; (iii) oriented attachment of the Bi–Te alloy particles into hexagonal platelets consisting of single crystalline inner spaces terminated by polycrystalline hexagonal frames, and (iv) the formation of whole single crystal hexagonal platelets after the hexagonal frames evolve into single crystalline through an oriented attachment process.[77]

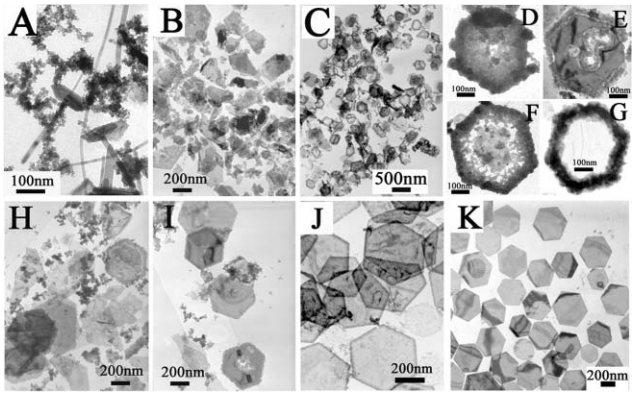


**Fig. 16** Typical TEM images of the time-dependent morphologies during the formation of $Bi_2Te_3$ hexagonal platelets: (A) 20 min, (B) 60 min, (C–I) 100 min, (J) 160 min, (K) 240 min.[77]

This study is helpful to design the solution phase synthesis of nanoarchitectures for materials possessing similar intrinsic crystal symmetries and could be extended to other material systems.

## 3. Thermoelectric properties of V-VI related nanostructures

It is generally accepted that nanostructures including nanowires, nanotubes and heterostructure nanowires provide alternative approaches to improve the TE conversion efficiency through size and interface effects on the transport properties of electrons and phonons. In this section, we try to briefly introduce the TE properties of the V-VI related nanostructures, including an individual nanowire, thin films and bulk nanocomposites composed of various nanostructures.

### 3.1 Thermoelectric properties of an individual nanowire

Although it is predicted that a very high $ZT$ value could be reached in the Bi-based nanowires, the measurement of an individual nanowire of each kind of material meets various challenges due to the rigorous demands for the thermal characterization microdevices. Along with the advance of the micro-processing techniques, there have also been some studies on the TE property measurements for an individual nanowire.[2,78-81]

Heath's group carried out a reliable four-point measurement of electrical-conductivity and TE power factor for polycrystalline Bi nanowires with different diameters after they successfully solved several key points by developing a more reasonable device architecture, which is clearly described in previous literature.[80] However, the resulting data indicated no obvious enhancement in the TE power factor due probably to the polycrystalline nature of the nanowires and the relatively large diameter of the Bi nanowires. Therefore, TE measurement of single crystalline thin Bi nanowires will be quite interesting and meaningful.

Shi's group has been devoted to this area for years and built a TE property measurement device for individual nanowires with the microelectromechanical system (MEMS) technique, as shown in Fig. 17.[82] Using this device, they successfully carried out the four-probe measurements for the thermal transport properties of a single $Bi_xTe_{1-x}$ nanowire synthesized through

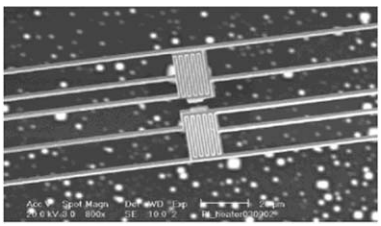

**Fig. 17** SEM image of the MEMS device for thermal characterization of 1D nanostructures.[82]

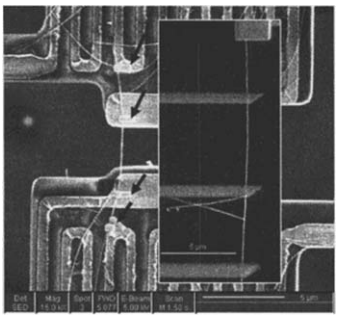

**Fig. 18** SEM of a $Bi_xTe_{1-x}$ nanowire trapped on the two suspended membranes of the measurement device. Four Pt lines were deposited locally on the nanowire, as labeled by the arrows. The inset is the SEM of another $Bi_xTe_{1-x}$ nanowire deposited on an oxidized silicon wafer and contacted by four Pt lines.[81]

galvanic electrodeposition.[81] Fig. 18 gives a typical SEM image of a $Bi_xTe_{1-x}$ nanowire trapped on the two suspended membranes of the measurement device. Four Pt lines were deposited locally on the nanowires, as labeled by the arrows. The results shown in Fig. 19 indicate that for $Bi_xTe_{1-x}$ nanowires with $x \approx 0.46$, the Seebeck coefficient ($S$) was 15–60% higher, and the electrical conductivity ($\sigma$) was close to the corresponding bulk values. In addition, they observed signatures of the increased phonon-boundary scattering that should reduce the lattice thermal conductivity, which suggests that a high $ZT$ can potentially be obtained in $Bi_xTe_{1-x}$ nanowires with an optimized atomic ratio.

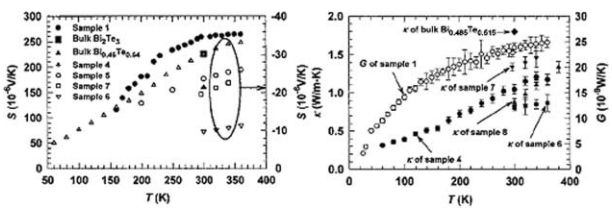


**Fig. 19** Seebeck coefficient (left) and thermal conductivity (right) as a function of temperature for the individual $Bi_xTe_{1-x}$ nanowire.[81]

The reliability and reproducibility of TE measurements on single nanowires needs further improvement, especially for thin nanowires, because the thermal stability of the nanowire, the precise control and measurement of temperature gradient along the nanowire, and the influence of thermal energy during the measurement, will influence the data.

 

### 3.2 Thermoelectric properties of nanostructured thin films

Because it is relatively hard to measure the TE properties of an individual nanowire/tube, there were some reports on estimating the TE properties of various nanostructures through building thin films with the as-prepared nanostructures. This route has advantages such as being cost effective and easy processing for the film formation, which to some extent is acceptable to assess the performance of the nanostructure.

Ramanath's group measured the room temperature electrical conductivity and Seebeck coefficient of the 350 °C annealed film consisting of randomly aligned $Bi_2Te_3$ nanorods synthesized with thioglycolic acid.[33] They built nanorod films by deposition through drop-casting techniques from dispersed $Bi_2Te_3$ nanorod solutions on a glass substrate connected to a microheater and microelectrodes for the property characterizations.[30] The electrical conductivity is estimated to be about 600 $\Omega^{-1}$ m$^{-1}$, a value approximately two orders of magnitude smaller than that of the bulk $Bi_2Te_3$. The negative Seebeck coefficient with a value of 100 μV K$^{-1}$ indicates the n-type semiconductor behavior due possibly to the sulfur doping during the sample preparation. In addition, the TE property of the $Sb_2Te_3$ platelets film was also studied.[75] The nanostructured film was prepared by dropping the as-prepared hexagonal platelets dispersed in aqueous solution onto an insulator, as shown in the left inset of Fig. 20. The electrical conductivity at the room temperature is estimated as 110 $\Omega^{-1}$ m$^{-1}$ which is lower than that of the bulk $Sb_2Te_3$, and the Seebeck coefficient approximately equals to 125 μV K$^{-1}$ (Fig. 20) which is about 1.6 times higher than that of the bulk crystals.

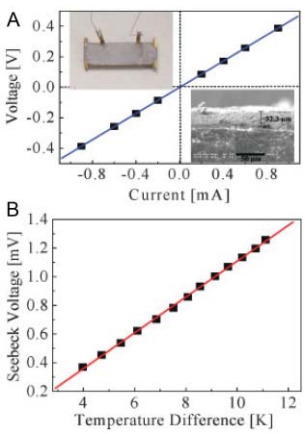


**Fig. 20** (A) $I$–$V$ characteristics from a TE film consisting of $Sb_2Te_3$ platelets. Left inset: optical photograph of a device with $Sb_2Te_3$ platelets film. Right inset: SEM image of the film in edge view showing the thickness of 32.3 μm. (B) Seebeck voltage-temperature difference relation of the two ends of device with the film.[75]

Different from the above mentioned studies that built the film through the redispersion of the obtained nanostructures, Chen's group directly obtained the ordered $Bi_2S_3$ nanorods film on a silicon wafer with a wet chemical route, which was prepared by mixing 10 ml of $Bi(NO_3)_3$ solution (0.05 M), and 60 ml of thiourea (Tu) solution (0.05M) in an acidic bath solution.[83] It should be noted that there is an insulative oxidized layer on the surface of the $Bi_2S_3$ nanorods, on which self assembled monolayers (SAMs) of 3-mercaptopropyl trimethoxysilane (MPTMS), which means that this approach is actually substrate independent by altering different SAMs for various substrates.[83] They then measured the thermoelectric properties of the self-assembled $Bi_2S_3$ nanorods film, as shown in Fig. 21. The electrical conductivity of the assembled $Bi_2S_3$ film at 300 K is as high as 5000 $\Omega^{-1}$ m$^{-1}$, which is much higher than those of other $Bi_2S_3$ films and that of bulk $Bi_2S_3$.[83] More important, the Seebeck coefficient reaches −755 μV K$^{-1}$ at 300 K, whose value is twice higher than that of bulk $Bi_2S_3$. The possible reasons for the enhanced TE transport properties of the film may be derived from the highly crystalline and c-axis oriented nature of the $Bi_2S_3$ nanorods.

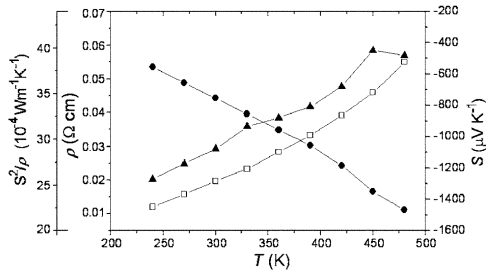


**Fig. 21** Temperature dependencies of the electrical resistivity (□), the Seebeck coefficient (●), and the thermoelectric power factor (▲) for the assembled $Bi_2S_3$ nanorods film on the MPTMS SAMs.[83]

### 3.3 Thermoelectric properties of bulk nanocomposites

Bulk nanocomposites provide a promising approach to reduce the thermal conductivity more than the electrical conductivity by interface scattering and to increase Seebeck coefficient enhancement more than decreasing the electrical conductivity, which is helpful for optimizing the $ZT$ value. Nanocomposite TE materials provide a promising approach for preparing a variety of desired shapes for device applications and scaled up to commercial markets. There have been both theoretical and experimental results on the TE properties of nanocomposites for various materials. In this section, we will briefly introduce the recent advance on studying the TE properties of the V-VI related nanocomposites composed of nanotubes and heterostructure nanowires.

Zhao *et al.* studied the effect of hydrothermally synthesized $Bi_2Te_3$ nanotubes on optimizing thermoelectric performances. They firstly grinded the zone-melted commercial n-type $Bi_2Te_3$ ingot into particles with diameters of about 100 nm and then mixed with the as-synthesized $Bi_2Te_3$ nanotubes with different weight ratios. The bulk sample was obtained through hot press process in vacuum at 350 °C for 30 min through a pressure of 50 MPa.[43] The thermal transport properties indicate that the nanocomposites possess a lower thermal conductivity (~1 W m$^{-1}$ K) and enhanced $ZT$ value as compared with the bulk $Bi_2Te_3$. Thus, it is worth expecting that a further optimization on TE properties could be obtained in the nanocomposites composed of the pure $Bi_2Te_3$ nanotubes with high crystallinity. To achieve this goal, our group studied the thermal transport properties of the bulk sample made of single crystalline $Bi_2Te_3$ nanotubes ($B_{NT}$) obtained through the solution phase nanoscale Kirkendall effect.[45] The bulk sample was made through a room temperature isostatic pressuring process with a pressure of 300 MPa for 20 min. As shown in Fig. 22, the Seebeck coefficient of the $B_{NT}$ is negative

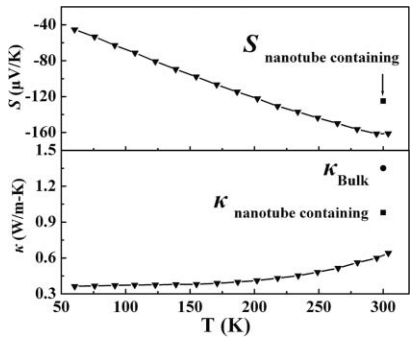


**Fig. 22** Seebeck coefficient and thermal conductivity of the $B_{NT}$ measured at a temperature range from 50 to 300 K. The data of bulk $Bi_2Te_3$ (●) and $Bi_2Te_3$ nanotube containing composites (■) come from Ref. 4 and 43, respectively.[45]

and increases almost linearly and reaches about −160 $\mu$V K$^{-1}$ at 300 K, which is larger than the $Bi_2Te_3$ nanotube-containing composites.[43] In addition, the thermal conductivity about 0.65 W m$^{-1}$ K$^{-1}$ at 300 K is much lower than these of $Bi_2Te_3$ bulk sample and $Bi_2Te_3$ nanotube-containing composites. It is evident that the enhanced Seebeck coefficient and greatly reduced thermal conductivity make strongly contributions to the improvement of the TE performance. However, the electrical resistivity ($\rho$) about $2.2 \times 10^{-4}$ Ω m at 300 K is tens of times larger than that of $Bi_2Te_3$ bulk due to the grain boundaries formed in $B_{NT}$. Therefore, the influence of grain boundaries on the transport properties can't be excluded and more investigation on the TE property is still needed in future. Despite this, the enhanced $ZT$ value in $B_{NT}$ could be possible if one can make high density bulk samples with pure $Bi_2Te_3$ nanotubes through some techniques, such as sparking plasma sintering (SPS) process.[84-86]

There are limited reports on the TE performance of the V-VI heterostructure nanowire composites due to the difficulty for the large-scale synthesis of the related products. Until now, only the study on the TE property on Te/Bi core/shell nanowire composites was reported.[72] We firstly built the Te/Bi core/shell nanowire powder into cuboid shape under a pressure of 10 MPa at room temperature and then further pressed through an isostatic pressing process with a pressure of 300 MPa for 20 min in order to reduce the porosity density. Compared with those of bulk Bi, both the Seebeck coefficient and thermal conductivity of the nanocomposites were greatly optimized, as shown in Fig. 23.[72] The Seebeck coefficient of the nanocomposites is about −128 mV K$^{-1}$ at 300 K, which is much higher than those of the conventional Bi nanowires or films (−22 to −28 mV K$^{-1}$). The thermal conductivity of about 0.55 W m$^{-1}$ K at 300 K is 15 times lower than that of the Bi bulk counterpart (8 W m$^{-1}$ K) probably due to the increased phonon scattering in the heterostructure nanowires with small diameters (20–25 nm) and thin shell thickness (2–5 nm). However, the $ZT$ value of the Te/Bi core/shell nanowire composites at 300 K is only about 0.05 because of the reduced electrical conductivity of about 100 times compared with that of the Bi bulk counterpart as a result of the present interface scattering of the nanowire composites.

Therefore, the most challenging issue for nanocomposites is to build high quality bulk samples with high density while simultaneously keeping the nanostructure feature in order to reach

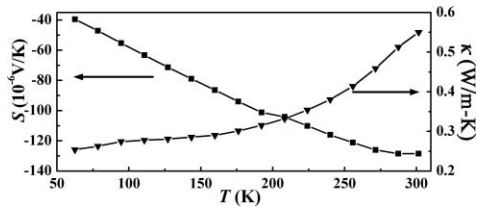


**Fig. 23** Seebeck coefficient and thermal conductivity of the bulk composites made of the Te/Bi core/shell heterostructure nanowires measured at a temperature range from 50 to 300 K.[72]

a high electrical conductivity close to the corresponding bulk counterpart and a largely reduced thermal conductivity.

## 4. Summary and Outlook

In this perspective, we have mainly described recent advances in V-VI related 1D nanostructures, including nanowires, nanotubes and heterostructures, and 2D platelet-like structures through electrodeposition and solution phase methods, followed by introducing the related research on the TE properties of both an individual nanowire and bulk nanocomposites consisting of these nanostructures.

The two synthetic routes have respective advantages and could be reciprocal for the synthesis of various V-VI nanostructures. For the fabrication of high quality V-VI nanowires and axial modulated 1D heterostructures, electrodeposition into the porous template is a dominate route, although there have been some studies on the solution phase synthesis of V-VI nanowires. For the synthesis of nanotubes, both electrodeposition and solution phase methods have moderately developed and some V-VI nanotubes were obtained recently. However, it is still a challenge for the synthesis of radial modulated heterostructure nanowires, and there have been limited reports on this topic through solution epitaxial growth process, where much effort should be devoted.

Efforts on the development of various synthetic routes for high quality V-VI nanostructures aim to enhance the TE performance for scalable applications of this class of material. However, there is little surprising outcome on TE property investigations of the single nanowire/tube, or bulk nanocomposites for chemically synthesized V-VI nanostructures. Actually, the TE property measurements of single nanowires encounters various challenges, including reliability and reproducibility of the results possibly derived from the device architecture, the underestimate of the thermal power because of the small nanowire diameters, the influence of variable melting points with decreased sizes and so on. Although there has been moderate progress on the TE property studies of single nanowires, much effort needs to be devoted. For nanostructured films and bulk nanocomposites, it could be possible to achieve enhanced TE performances after great quality improvement of the nanostructured products. In general, the Seebeck coefficient and thermal conductivity of the films and bulk nanocomposites will be notably optimized. However, the electrical conductivity of the nanostructured films and bulk nanocomposites could be much lower as compared with their corresponding bulk materials due to the insufficient contact or the influence of the grain boundaries or the interface scattering during the formation of film or nanocomposite structures by deposition or pressure, which will greatly diminish the $ZT$ value of the

 

sample. Therefore, the most challenging step is how to build high quality films or bulk samples with various nanostructures through modified techniques in order to get a high electrical conductivity while keeping the lowered thermal conductivity derived from the nanostructure feature.

It is true that there are still difficulties in the development of V-VI nanostructures, especially the enhancement of the *ZT* value. However, we believe that, along with the advance of the related techniques including the powerful synthetic routes, precise micro-processing techniques, optimized bulk sample preparation processes, *etc*., there will be significant progress in both the chemical synthesis and TE property enhancement of V-VI related nanostructures in the near future.



## Acknowledgements

This work was supported by the National Natural Science Foundation of China (Grant Nos. 50721061 and 50832007) and the National Basic Research Program of China (Grant Nos. 2006CB922005 and 2009CB929502).

## References

1 L. E. Bell, *Science*, 2008, **321**(5895), 1457–1461.
2 A. I. Hochbaum, R. K. Chen, R. D. Delgado, W. J. Liang, E. C. Garnett, M. Najarian, A. Majumdar and P. D. Yang, *Nature*, 2008, **451**(7175), 163–U5.
3 F. J. DiSalvo, *Science*, 1999, **285**(5428), 703–706.
4 D. M. Rowe, *CRC Handbook of Thermoelectrics*, CRC, Boca Raton, 1995.
5 M. S. Dresselhaus, G. Chen, M. Y. Tang, R. G. Yang, H. Lee, D. Z. Wang, Z. F. Ren, J. P. Fleurial and P. Gogna, *Adv. Mater.*, 2007, **19**(8), 1043–1053.
6 B. C. Sales, *Science*, 2002, **295**(5558), 1248–1249.
7 R. Venkatasubramanian, E. Siivola, T. Colpitts and B. O'Quinn, *Nature*, 2001, **413**(6856), 597–602.
8 H. Bottner, G. Chen and R. Venkatasubramanian, *MRS Bull.*, 2006, **31**(3), 211–217.
9 Y. G. Wang, X. F. Xu and R. Venkatasubramanian, *Appl. Phys. Lett.*, 2008, **93**(11).
10 L. D. Hicks and M. S. Dresselhaus, *Phys. Rev. B: Condens. Matter*, 1993, **47**(24), 16631–16634.
11 I. Bejenari and V. Kantser, *Phys. Rev. B: Condens. Matter Mater. Phys.*, 2008, **78**(11), 115322.
12 L. D. Hicks, T. C. Harman, X. Sun and M. S. Dresselhaus, *Phys. Rev. B: Condens. Matter*, 1996, **53**(16), R10493–10496.
13 S. A. Sapp, B. B. Lakshmi and C. R. Martin, *Adv. Mater.*, 1999, **11**(5), 402–404.
14 A. L. Prieto, M. S. Sander, M. Martin-Gonzalez, R. Gronsky, T. Sands and A. M. Stacy, *J. Am. Chem. Soc.*, 2001, **123**(29), 7160–7161.
15 M. S. Sander, A. L. Prieto, R. Gronsky, T. Sands and A. M. Stacy, *Adv. Mater.*, 2002, **14**(9), 665–667.
16 M. S. Sander, R. Gronsky, T. Sands and A. M. Stacy, *Chem. Mater.*, 2003, **15**(1), 335–339.
17 C. G. Jin, G. W. Jiang, W. F. Liu, W. L. Cai, L. Z. Yao, Z. Yao and X. G. Li, *J. Mater. Chem.*, 2003, **13**(7), 1743–1746.
18 C. G. Jin, X. Q. Xiang, C. Jia, W. F. Liu, W. L. Cai, L. Z. Yao and X. G. Li, *J. Phys. Chem. B*, 2004, **108**(6), 1844–1847.
19 C. G. Jin, G. Q. Zhang, T. Qian, X. G. Li and Z. Yao, *J. Phys. Chem. B*, 2005, **109**(4), 1430–1432.
20 J. Lee, S. Farhangfar, J. Lee, L. Cagnon, R. Scholz, U. Gosele and K. Nielsch, *Nanotechnology*, 2008, **19**(36), 365701.
21 M. Martin-Gonzalez, A. L. Prieto, R. Gronsky, T. Sands and A. M. Stacy, *Adv. Mater.*, 2003, **15**(12), 1003.
22 M. Martin-Gonzalez, G. J. Snyder, A. L. Prieto, R. Gronsky, T. Sands and A. M. Stacy, *Nano Lett.*, 2003, **3**(7), 973–977.
23 F. Xiao, B. Y. Yoo, K. H. Lee and N. S. V. Myung, *Nanotechnology*, 2007, **18**(33), 335203.
24 C. Burda, X. B. Chen, R. Narayanan and M. A. El-Sayed, *Chem. Rev.*, 2005, **105**(4), 1025–1102.
25 M. Niederberger, *Acc. Chem. Res.*, 2007, **40**(9), 793–800.
26 I. U. Arachchige and S. L. Brock, *Acc. Chem. Res.*, 2007, **40**(9), 801–809.
27 X. Wang, Q. Peng and Y. D. Li, *Acc. Chem. Res.*, 2007, **40**(8), 635–643.
28 X. Wang and Y. D. Li, *Inorg. Chem.*, 2006, **45**(19), 7522–7534.
29 H. Yu, P. C. Gibbons and W. E. Buhro, *J. Mater. Chem.*, 2004, **14**(4), 595–602.
30 F. D. Wang, R. Tang, H. Yu, P. C. Gibbons and W. E. Buhro, *Chem. Mater.*, 2008, **20**(11), 3656–3662.
31 J. W. Wang, X. Wang, C. Peng and Y. D. Li, *Inorg. Chem.*, 2004, **43**(23), 7552–7556.
32 Y. W. Wang and K. S. Kim, *Nanotechnology*, 2008, **19**(26).
33 A. Purkayastha, F. Lupo, S. Kim, T. Borca-Tasciuc and G. Ramanath, *Adv. Mater.*, 2006, **18**(4), 496.
34 T. Sun, X. B. Zhao, T. J. Zhu and J. P. Tu, *Mater. Lett.*, 2006, **60**(20), 2534–2537.
35 R. G. Yang, G. Chen and M. S. Dresselhaus, *Phys. Rev. B: Condens. Matter Mater. Phys.*, 2005, **72**(12), 125418.
36 R. G. Yang, G. Chen and M. S. Dresselhaus, *Nano Lett.*, 2005, **5**(6), 1111–1115.
37 L. Li, Y. H. Xiao, Y. W. Yang, X. H. Huang, G. H. Li and L. D. Zhang, *Chem. Lett.*, 2005, **34**(7), 930–931.
38 L. Li, Y. W. Yang, X. H. Huang, G. H. Li, R. Ang and L. D. Zhang, *Appl. Phys. Lett.*, 2006, **88**(10).
39 D. C. Yang, G. W. Meng, Q. L. Xu, F. M. Han, M. G. Kong and L. D. Zhang, *J. Phys. Chem. C*, 2008, **112**(23), 8614–8616.
40 X. H. Li, B. Zhou, L. Pu and J. J. Zhu, *Cryst. Growth Des.*, 2008, **8**(3), 771–775.
41 Y. D. Li, J. W. Wang, Z. X. Deng, Y. Y. Wu, X. M. Sun, D. P. Yu and P. D. Yang, *J. Am. Chem. Soc.*, 2001, **123**(40), 9904–9905.
42 H. M. Cui, H. Liu, X. Li, J. Y. Wang, F. Han, X. D. Zhang and R. I. Boughton, *J. Solid State Chem.*, 2004, **177**(11), 4001–4006.
43 X. B. Zhao, X. H. Ji, Y. H. Zhang, T. J. Zhu, J. P. Tu and X. B. Zhang, *Appl. Phys. Lett.*, 2005, **86**(6).
44 F. Xiao, B. Yoo, K. H. Lee and N. V. Myung, *J. Am. Chem. Soc.*, 2007, **129**(33), 10068–10069.
45 G. Q. Zhang, Q. X. Yu, Z. Yao and X. G. Li, *Chem. Commun.*, 2009, 2317–2319.
46 X. Wang, J. Zhuang, Q. Peng and Y. D. Li, *Nature*, 2005, **437**(7055), 121–124.
47 X. L. Lu, G. Q. Zhang, W. Wang and X. G. Li, *Angew. Chem., Int. Ed.*, 2007, **46**(30), 5772–5774.
48 Y. D. Yin, R. M. Rioux, C. K. Erdonmez, S. Hughes, G. A. Somorjai and A. P. Alivisatos, *Science*, 2004, **304**(5671), 711–714.
49 Y. D. Yin, C. Erdonmez, S. Aloni and A. P. Alivisatos, *J. Am. Chem. Soc.*, 2006, **128**(39), 12671–12673.
50 X. Liang, X. Wang, Y. Zhuang, B. Xu, S. M. Kuang and Y. D. Li, *J. Am. Chem. Soc.*, 2008, **130**(9), 2736–2377.
51 C. M. Lieber and Z. L. Wang, *MRS Bull.*, 2007, **32**(2), 99–108.
52 A. J. Mieszawska, R. Jalilian, G. U. Sumanasekera and F. P. Zamborini, *Small*, 2007, **3**(5), 722–756.
53 J. Q. Hu, Y. Bando and D. Golberg, *J. Mater. Chem.*, 2009, **19**(3), 330–343.
54 Y. Wu, J. Xiang, C. Yang, W. Lu and C. M. Lieber, *Nature*, 2004, **430**(6995), 61–65.
55 Y. Huang, X. F. Duan, Y. Cui, L. J. Lauhon, K. H. Kim and C. M. Lieber, *Science*, 2001, **294**(5545), 1313–1317.
56 M. S. Gudiksen, L. J. Lauhon, J. Wang, D. C. Smith and C. M. Lieber, *Nature*, 2002, **415**(6872), 617–620.
57 L. J. Lauhon, M. S. Gudiksen, C. L. Wang and C. M. Lieber, *Nature*, 2002, **420**(6911), 57–61.
58 F. Qian, Y. Li, S. Gradecak, D. L. Wang, C. J. Barrelet and C. M. Lieber, *Nano Lett.*, 2004, **4**(10), 1975–1979.
59 Y. M. Lin and M. S. Dresselhaus, *Phys. Rev. B: Condens. Matter Mater. Phys.*, 2003, **68**(7), 075304.
60 R. Prasher, *Appl. Phys. Lett.*, 2006, **89**(6), 063121.
61 F. H. Xue, G. T. Fei, B. Wu, P. Cui and L. D. Zhang, *J. Am. Chem. Soc.*, 2005, **127**(44), 15348–15349.
62 X. C. Dou, G. H. Li and H. C. Lei, *Nano Lett.*, 2008, **8**(5), 1286–1290.
63 B. Yoo, F. Xiao, K. N. Bozhilov, J. Herman, M. A. Ryan and N. V. Myung, *Adv. Mater.*, 2007, **19**(2), 296.
64 W. Wang, G. Q. Zhang and X. G. Li, *J. Phys. Chem. C*, 2008, **112**(39), 15190–15194.

65 W. Wang, X. L. Lu, T. Zhang, G. Q. Zhang, W. J. Jiang and X. G. Li, *J. Am. Chem. Soc.*, 2007, **129**(21), 6702–6703.
66 W. Wang, G. Q. Zhang and X. G. Li, *Chem. Lett.*, 2008, **37**(8), 848–849.
67 R. D. Robinson, B. Sadtler, D. O. Demchenko, C. K. Erdonmez, L. W. Wang and A. P. Alivisatos, *Science*, 2007, **317**(5836), 355–358.
68 D. V. Talapin, J. H. Nelson, E. V. Shevchenko, S. Aloni, B. Sadtler and A. P. Alivisatos, *Nano Lett.*, 2007, **7**(10), 2951–2959.
69 L. Ouyang, K. N. Maher, C. L. Yu, J. McCarty and H. Park, *J. Am. Chem. Soc.*, 2007, **129**(1), 133–138.
70 A. G. Dong, F. D. Wang, T. L. Daulton and W. E. Buhro, *Nano Lett.*, 2007, **7**(5), 1308–1313.
71 W. G. Lu, Y. Ding, Y. X. Chen, Z. L. Wang and J. Y. Fang, *J. Am. Chem. Soc.*, 2005, **127**(28), 10112–10116.
72 G. Q. Zhang, W. Wang and X. G. Li, *Adv. Mater.*, 2008, **20**(19), 3654.
73 S. S. Garje, D. J. Eisler, J. S. Ritch, M. Afzaal, P. O'Brien and T. Chivers, *J. Am. Chem. Soc.*, 2006, **128**(10), 3120–3121.
74 W. Z. Wang, B. Poudel, J. Yang, D. Z. Wang and Z. F. Ren, *J. Am. Chem. Soc.*, 2005, **127**(40), 13792–13793.
75 W. D. Shi, L. Zhou, S. Y. Song, J. H. Yang and H. J. Zhang, *Adv. Mater.*, 2008, **20**(10), 1892.
76 B. Zhou, Y. Ji, Y. F. Yang, X. H. Li and J. H. Zhu, *Cryst. Growth Des.*, 2008, **8**(12), 4394–4397.
77 G. Q. Zhang, W. Wang, X. L. Lu and X. G. Li, *Cryst. Growth Des.*, 2009, **9**(1), 145–150.
78 A. I. Boukai, Y. Bunimovich, J. Tahir-Kheli, J. K. Yu, W. A. Goddard and J. R. Heath, *Nature*, 2008, **451**(7175), 168–171.
79 C. H. Yu, L. Shi, Z. Yao, D. Y. Li and A. Majumdar, *Nano Lett.*, 2005, **5**(9), 1842–1846.
80 A. Boukai, K. Xu and J. R. Heath, *Adv. Mater.*, 2006, **18**(7), 864.
81 J. H. Zhou, C. G. Jin, J. H. Seol, X. G. Li and L. Shi, *Appl. Phys. Lett.*, 2005, **87**(13).
82 L. Shi, C. H. Yu and J. H. Zhou, *J. Phys. Chem. B*, 2005, **109**(47), 22102–22111.
83 S. C. Liufu, L. D. Chen, Q. Yao and C. F. Wang, *Appl. Phys. Lett.*, 2007, **90**(11).
84 C. Recknagel, N. Reinfried, P. Hohn, W. Schnelle, H. Rosner, Y. Grin and A. Leithe-Jasper, *Sci. Tech. Adv. Mater.*, 2007, **8**(5), 357–363.
85 W. S. Liu, B. P. Zhang, J. F. Li, H. L. Zhang and L. D. Zhao, *J. Appl. Phys.*, 2007, **102**(10).
86 L. D. Zhao, B. P. Zhang, W. S. Liu and J. F. Li, *J. Appl. Phys.*, 2009, **105**(2).



 